



LETTER • OPEN ACCESS

Active percolation in pusher-type microswimmers

To cite this article: Fabian Jan Schwarzendahl and Marco G. Mazza 2022 *EPL* **140** 47001

View the [article online](#) for updates and enhancements.

You may also like

- [Physics of microswimmers—single particle motion and collective behavior: a review](#)
J Elgeti, R G Winkler and G Gompper
- [Simulation of microswimmer hydrodynamics with multiparticle collision dynamics](#)
Andreas Zöttl
- [Microswimmers in an axisymmetric vortex flow](#)
José-Agustín Arguedas-Leiva and Michael Wilczek

Active percolation in pusher-type microswimmers

FABIAN JAN SCHWARZENDAHL^{1,2,3}  and MARCO G. MAZZA^{3,4(a)} 

¹ *Institut für Theoretische Physik II: Weiche Materie, Heinrich-Heine-Universität Düsseldorf
40225 Düsseldorf, Germany*

² *Department of Physics, University of California - Merced, 5200 N. Lake Road, Merced, CA 95343, USA*

³ *Max Planck Institute for Dynamics and Self-Organization (MPIDS) - Am Faßberg 17, 37077 Göttingen, Germany*

⁴ *Interdisciplinary Centre for Mathematical Modelling and Department of Mathematical Sciences,
Loughborough University - Loughborough, Leicestershire LE11 3TU, UK*

received 29 July 2021; accepted in final form 8 November 2022
published online 22 November 2022

Abstract – The aggregation of microorganisms in colonies and biofilms underpins a myriad of biological processes, and has crucial implications in ecology and biomedical sciences. While much of our knowledge of microbial motion is based on single-cell mechanisms or cell-cell interactions, the origin of cooperativity in microbial communities is not yet fully understood. Here, we reveal the existence of a continuum percolation transition in two model suspensions of pusher-type microswimmers: an asymmetric dumbbell and a squirmer model. Clusters of swimmers held together by hydrodynamic forces dynamically aggregate and separate. Using simulations with explicit hydrodynamics and theory, we find that as the microswimmers' filling fraction increases, the cluster size distribution approaches a scale-free form and system-spanning clusters emerge.



Copyright © 2022 The author(s)

Published by the EPLA under the terms of the [Creative Commons Attribution 4.0 International License](https://creativecommons.org/licenses/by/4.0/) (CC BY). Further distribution of this work must maintain attribution to the author(s) and the published article's title, journal citation, and DOI.

Introduction. – The collective organization and aggregation of suspensions of microorganisms such as bacteria or microalgae plays a crucial role in bacterial aggregates [1], biofilms [2], and phytoplankton flocculation [3,4]. Microbial aggregation is a striking result of the concurrence of physical and biological forces [5,6], with important implications such as wastewater management [7,8], biomedical treatments [9], or the marine food webs [3]. Extensive investigations have shown that effects such as self-concentration [10,11], swarming [12], spontaneous formation of spiral vortices [13] and of fluid flows [14], bacterial turbulence [15], and biofilms [16] are strongly correlated effects. Invariably, microbial motion takes place in an aqueous environment. Although the long-ranged nature of hydrodynamic interactions among swimming cells is often recognized [17–23] as naturally forming the backbone of collective effects, it is still not fully understood how self-organization emerges from correlations. Recent theoretical [24–28] and experimental works [29–33] have found evidence of concentration

fluctuations and dynamical transitions to clustered states. A particularly interesting route to aggregation is the percolation transition, indications thereof have been seen in c-shaped active Brownian particles [25], eukaryotic cells [34], and at the onset of mesoscale turbulence [35].

Here, we combine particle-based computer simulations which include explicit hydrodynamic interactions, and theoretical arguments with methods put forward in [11] to study a bulk suspension of microswimmers. In order to investigate the generality of our results, we study two model swimmers differing in shape: asymmetric dumbbells and spherical squirmers. These models, though they include some simplifications, are analytically tractable and can provide some insight into the underlying physics; we also study the Fokker-Planck equation of our system and find an instability leading to the growth of density fluctuations at the same average concentration as found in the simulations. In this work, we find that our model microswimmers form dynamic aggregates, held together by hydrodynamic interactions, and that upon increasing the suspension's filling fraction undergo a percolation transition. We verify that, properly applied, some classical

^(a)E-mail: m.g.mazza@lboro.ac.uk (corresponding author)

concepts from percolation theory [36] such as scaling laws and critical exponents can be used to characterize this active percolation transition.

Simulation methods. – We consider a suspension of pusher-type microswimmers, such as the bacteria *Escherichia coli*. We employ a stroke-averaged biological microswimmer model, consisting of an asymmetric dumbbell, which represents the swimmer’s body and fore-aft asymmetry [11,37–39], see fig. S1 in the Supplementary Material `SupplementaryMaterial.pdf` (SM) (similarly shaped phoretic microswimmers were studied in [40,41]). The dynamics of this dumbbell-shaped swimmers are governed by Newton’s equations of motion [11]. As the swimmer is asymmetric in shape, the hydrodynamic center is shifted away from the center of mass of the swimmer, which enables the swimmers’ propulsion. Hydrodynamic interactions generally depend on shape [42]. In order to investigate the generality of our results, we also consider a pusher-type squirmer model [43,44], differing in both shape and propulsion mechanism from the dumbbell model, to test the robustness of our results; see SM, sect. V. Note that we do not include details of the swimmer’s flagella and synchronization effects [45,46].

Experiments [47] have shown that the hydrodynamic flow field of the pusher-type swimmer *E. coli* corresponds to a force dipole. The hydrodynamic flow field generated by each microswimmer induces interactions which play a key role in the microswimmers’ collective behavior [18,48–50]. Furthermore, no-slip boundary conditions are implemented on the dumbbell-shaped swimmer’s body.

To resolve the hydrodynamic interactions numerically, we use the multiparticle collision dynamics (MPCD) technique. MPCD is a particle-based method accounting for hydrodynamic modes up to the Navier-Stokes level [51]. Specifically, we use the MPCD-at + A [52,53] technique, that has an Anderson thermostat which conserves the fluid’s temperature and conserves angular momentum; the latter is necessary to correctly account for rotations of the swimmers [53]. The MPCD fluid is characterized by its temperature T , MPCD particle mass m , and size of a MPCD grid cell a as a unit of length. In our simulations, the average number of MPCD particles in each MPCD cell $\langle N_C \rangle = 20$ and the timestep $\delta t = 0.01 \sqrt{ma^2/(k_B T)}$. The size of an individual swimmer is $\sigma \approx 5a$, which ensures an accurate calculation of small and large scale hydrodynamic effects. The repulsive steric interactions among swimmers are modeled using a Weeks-Chandler-Andersen potential [54] between each sphere of the dumbbells. In the simulations of squirmers, the particle diameter is $\sigma = 6a$. In all our simulations, we use a cubic domain with periodic boundary conditions and constant volume.

We perform simulations of the dumbbell swimmers in domains of linear size $L = 100a, 120a, 130a, 200a$. We vary the filling fraction of our system defined as $\phi = NV_{\text{sw}}/L^3$, where V_{sw} is the volume of an individual swimmer. In the small system ($L = 100a$) we simulate a

range of $N = 388\text{--}2300$ swimmers, corresponding to filling fractions from $\phi = 0.07$ to $\phi = 0.43$, while in the large system ($L = 200a$) we use $N = 3800\text{--}18200$, *i.e.*, from $\phi = 0.09$ to $\phi = 0.43$. The active state is characterized by the Péclet number $\mathcal{P} = v\sigma/D$, which compares the self-propulsion speed $v = 0.05 \sqrt{k_B T/m}$ (active transport) to the diffusive transport $D = 1.4 \times 10^{-4} a \sqrt{k_B T/m}$ of a microswimmer, and by the Reynolds number (measuring the ratio of inertial to viscous forces) $\mathcal{R} = \sigma v \rho / \eta$, where ρ is the fluids’ density and η is the fluid’s viscosity. The kinematic viscosity of our fluid is $\nu = 3.88a \sqrt{k_B T/m}$ and the rotational diffusion coefficient of a swimmer is $D_R = 4.1 \times 10^{-6} \sqrt{k_B T/(ma^2)}$ [11]. In our simulations of dumbbells, the Péclet number is $\mathcal{P} \approx 1.8 \times 10^3$ and the Reynolds number is $\mathcal{R} = 0.1$ (see the SM for additional results with $\mathcal{R} = 0.01$). We averaged over 3000 simulation configurations after the system reached a steady state. More details on our computational model can be found in [11] and the SM. For the squirmer simulations, the system size is $L = 130a$ and the number of swimmers is $N = 1800\text{--}8400$. We fix the Péclet number $\mathcal{P} = v_0 \sigma / D = 1.3 \times 10^3$ and the Reynolds number $\mathcal{R} = 0.08$.

To quantify the aggregation process, we perform a cluster analysis based on the interparticle distance, *i.e.*, if the center-of-mass distance of two swimmers is less than $r_{\text{cl}} = 1.5\sigma$, both particles are assigned to the same cluster (r_{cl} is the distance at which the radial distribution function crosses unity [55]; changes to r_{cl} within reasonable bounds do not affect our results; see the SM, sect. VII). Given a particle-based observable \mathcal{F}_i , we compute the *cluster average* $F(s) = \langle \frac{1}{s} \sum_i \mathcal{F}_i \rangle_{\text{clust}}$. To this end, i) we perform a cluster analysis, and identify the clusters present in the system; ii) we compute $s^{-1} \sum_i \mathcal{F}_i$ separately for each cluster; iii) we average the results only among homologous clusters, *i.e.*, clusters with the same size s .

Percolation of microswimmers. – Our model suspension consists of a large number of microswimmers in three dimensions. The apparently chaotic motion of the swimmers generates dynamical aggregates, that is, rather long-lived groups of particles in close proximity of each other. Figures 1(a)–(c) show typical, steady-state configurations of our pusher-type swimmers at three different filling fractions ϕ . The physical origin of the attractive forces holding together the particles are the long-ranged hydrodynamic interactions. Generally, pusher-type swimmers swimming side by side exert a hydrodynamic attraction on each other [45,56]. In absence of external fields, the presence of other swimmers produces a more complex texture of attractive and repulsive configurations [55].

Figures 1(a)–(c) show in different colors the resulting clusters for those configurations. These are dynamical clusters where particles easily join or leave a given cluster. As the filling fraction increases, clusters grow in size; at $\phi = 0.22$ we find clusters comparable with the linear size of the system. For $\phi \geq 0.26$, very large clusters (but

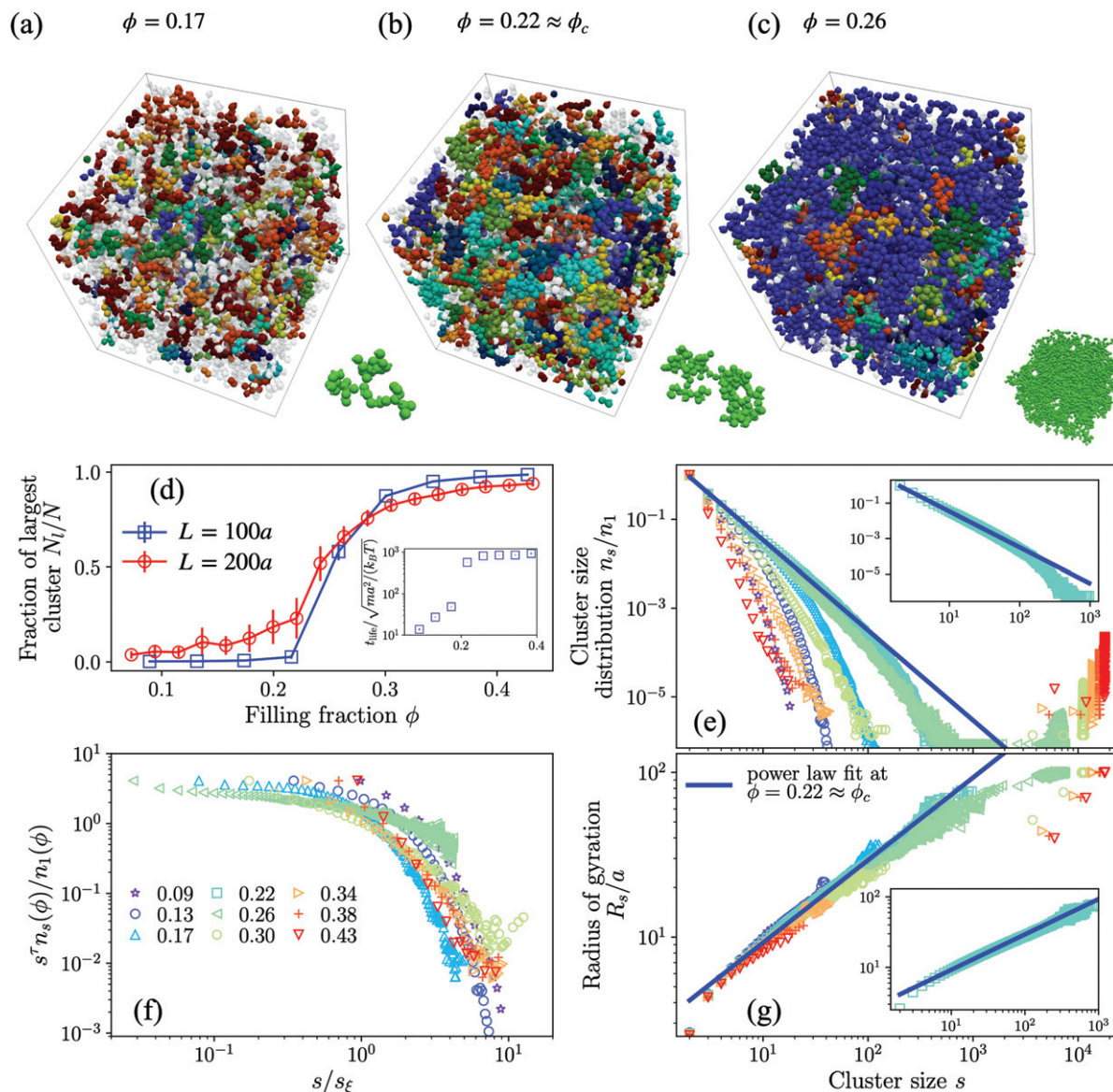


Fig. 1: Percolation and scaling properties of swimmers. (a)–(c) Example configurations of dumbbell swimmers at different filling fractions ($L = 200a$). Gray transparent particles do not belong to any cluster. Different colors correspond to different clusters. The system-spanning cluster at $\phi = 0.26$ is consistent with a percolation transition. On the bottom right of each configuration a zoom-in view of the largest cluster identified is shown. (d) Fraction of number of particles in the largest cluster to total number of particles N_l/N . Inset (d) shows the average cluster lifetime. (e) Cluster size distribution n_s normalized to the number of single-particle clusters n_1 for different filling fractions ($L = 200a$). The solid line is a fit to the data for $\phi = 0.22$, giving the Fisher exponent $\tau = 2.033 \pm 0.003$. The inset (e) shows the fitted data ($\phi = 0.22$) for the sake of clarity. (f) Collapse of the probability distribution to an exponential scaling function. (g) Radius of gyration for different filling fractions ($L = 200a$). The solid line is a fit to the data for $\phi = 0.22$, giving the fractal dimension $d_f = 1.99 \pm 0.02$. The inset shows the fitted data ($\phi = 0.22$) for the sake of clarity.

still dynamically rearranging) spanning the entire system emerge. In figs. 1(a)–(c) we also show the largest cluster found in each system displayed. We discuss below the fractal dimension of the clusters. We note that the clustering shown here is a result of hydrodynamic attractions between microswimmers, and is distinct from clustering mechanisms in dry active systems [57–59].

While it is clear that there are hydrodynamic attractions, it is not at all obvious that these attractive forces

should spread until the entire system is engulfed in a closely connected aggregate. Beyond the simple physical picture discussed above, more detailed models [48–50,60–62] reveal an instability of the orientational field. However, the concentration of swimmers is known to have important effects [18,63], that need to be taken into account.

Physical forces. – We now derive a Fokker-Planck description of our swimmer suspension to further understand

the origin of the clustering in relation to hydrodynamic interactions; see also the SM, sect. II. Microswimmers obey the following Langevin equations $\frac{d\mathbf{r}_{i\mu}}{dt} = \mathbf{u}(\mathbf{r}_{i\mu})$ where $i \in \{F, B\}$ refers to the front or back sphere of the μ -th swimmer, and \mathbf{u} is the velocity of the surrounding fluid. The fluid velocity \mathbf{u} evolves according to the Stokes equation, $\eta\nabla^2\mathbf{u} = \nabla P - \mathbf{f}^{\text{active}} + \mathbf{f}^{\text{noise}}$, where P is the pressure and η is the fluid's viscosity, $\mathbf{f}^{\text{active}} = \sum_{\mu=1}^N f\mathbf{e}_\mu [\delta(\mathbf{r} - \mathbf{r}_{F\mu}) - \delta(\mathbf{r} - \mathbf{r}_{B\mu})]$, where f is the strength of the dipole, $\mathbf{e}_\mu = (\mathbf{r}_{F\mu} - \mathbf{r}_{B\mu})/l$ is the orientation of the dumbbell, and $\delta(\mathbf{r} - \mathbf{r}_\mu)$ is the Dirac delta distribution, and $\mathbf{f}^{\text{noise}}$ are Gaussian white noises (see the SM).

The Fokker-Planck equation for the probability $p(\mathbf{r}, \mathbf{e}, t)$ to find a swimmer at position \mathbf{r} with orientation \mathbf{e} at time t reads

$$\begin{aligned} \frac{\partial}{\partial t} p = & -\nabla \cdot [v(c)\mathbf{e}p] - \frac{1}{\zeta_{hy}} \nabla \cdot (\mathbf{F}_{hy}p) + D\nabla^2 p \\ & - \frac{1}{\zeta_{hy}l^2} \left(\mathbf{e} \times \frac{\partial}{\partial \mathbf{e}} \right) \cdot \boldsymbol{\tau}_{hy} p + D_R \left(\mathbf{e} \times \frac{\partial}{\partial \mathbf{e}} \right)^2 p, \end{aligned} \quad (1)$$

where $v(c) \equiv v_0 - c\zeta$ models the steric interactions between swimmers, with the concentration of the swimmers c and the factor ζ controlling the strength of coupling to steric interactions. Furthermore, $v_0 = -f\Delta a/(8\pi\eta\bar{a})$ is the swimmers' self-propulsion speed, depending on the swimmer's average size $\bar{a} = (a_B + a_F)/2$ and shape anisotropy $\Delta a = (a_B - a_F)$, and length of the dumbbell l ; a_F , a_B are the radii of the front, back sphere of the dumbbell, respectively; D and D_R are the translational and rotational diffusion coefficients, respectively (see the SM, sect II for the definition of the hydrodynamic forces and torques in eq. (1)).

A linear stability analysis of the moments (concentration, polarization, and nematicity) including the coupling of steric effects with hydrodynamics in eq. (1) reveals that fluctuations in the swimmers' concentration $\delta\bar{c}$ become unstable; in Fourier space

$$\begin{aligned} \partial_t \delta\bar{c} = & -\omega(\theta_k) \frac{fl(v_0 - 2c_0\zeta)}{30\bar{a}\eta^2(v_0\zeta c_0)^2} \\ & \times [30\bar{a}\eta(v_0 - c_0\zeta) + c_0\Delta a fl^2] \delta\bar{c}. \end{aligned} \quad (2)$$

Here, $\omega(\theta_k) < 0$ for a broad range of values of the azimuthal angle θ_k of the wave vector \mathbf{k} . Furthermore, $f > 0$ for pushers, and c_0 is the average concentration. The term proportional to $\delta\bar{c}$ on the right-hand side of eq. (2) is positive in a broad range of swimmers' configurations, which indicates a growth of density fluctuations in the swimmers (see the SM, sect. II for analytical details). Both our simulations and analytical calculations show that the largest fluctuations in the density of microswimmers occur at filling fraction of approximately 0.2 (see the SM, sect. II and also [11]).

Scaling properties. – To scrutinize what the statistical importance of the active aggregates is, we compute

the percolation order parameter, *i.e.*, the fraction of the largest cluster, defined as the ratio between the number of particles belonging to the largest cluster N_l and the total number of particles in the system N . Figure 1(d) shows the steady-state fraction of the largest cluster N_l/N for varying filling fractions ϕ for two different system sizes. The fractional size of the largest cluster N_l/N is negligible at low ϕ , but beyond a threshold value $\phi_c \approx 0.22$ it increases continuously towards unity, indicating that the largest cluster occupies the entire system. This state of affairs is reminiscent of classical percolation, and N_l/N acts as an order parameter for the percolation transition.

To meaningfully speak of clusters, we compute their average lifetime t_{life} as follows. Given a cluster at time t_0 , if at least 7 of its member particles are still within the cutoff distance of our cluster definition at time t_1 then that cluster still lives at time t_1 . Lifetimes are calculated for all clusters with $s \geq 7$ particles, and averaged over all homologous clusters at a given ϕ . As a comparison, the average time an isolated swimmer need to travel its own body length is $100\sqrt{ma^2/(k_B T)}$. Figure 1(d) inset shows that the average t_{life} increases with ϕ and then approaches a finite value at the percolation transition. This asymptotic value at large filling fractions is dominated by the system-spanning cluster.

Percolation theory predicts a scale free probability distribution of cluster sizes at the critical point. We test this hypothesis by computing the distribution $n_s(s)$ of cluster sizes s . Figure 1(e) shows n_s for different ϕ . Although these clusters are dynamic in nature, and a given cluster may grow or shrink with time, the cluster size distribution is statistically stationary, that is, the distribution of clusters does not depend on time. As ϕ increases towards $\phi = 0.22$, the cluster size distribution $n_s(s)$ increasingly approaches a power-law form, indicating the absence of any characteristic length scale. Identifying $\phi_c = 0.22$ as the critical filling fraction (fig. 1(e) inset) we find $n_s(s)|_{\phi_c} \sim s^{-\tau}$, where $\tau \approx 2.033 \pm 0.003$ is the Fisher exponent [36] (hereinafter errors indicate standard deviation of the fit). These results are reminiscent of continuum percolation of colloids [64] or simple fluids [65], and confirm our hypothesis.

Away from ϕ_c , the theory predicts that

$$n_s(s) \sim s^{-\tau} \exp(-s/s_\xi), \quad (3)$$

where s_ξ is the cutoff cluster size. Equation (3) implies a non-monotonous behavior of the cluster distributions that is seen in fig. 1(e). We find s_ξ for each filling fraction by fitting the respective cluster size distribution in fig. 1(e) to eq. (3). In fig. 1(f) we plot $s^\tau n_s(\phi)/n_1(\phi)$ against s/s_ξ , which suggests a collapse of the data onto an exponential master curve, as predicted by eq. (3).

The geometrical features of the clusters can be described by their radius of gyration and fractal dimension. In fig. 1(g) we show the dependence of the radius of gyration $R_s^2(s) \equiv \langle \frac{1}{s} \sum_i (\mathbf{r}_i - \mathbf{r}_{\text{CoM}})^2 \rangle_{\text{clust}}$ on cluster size s for different filling fractions, where \mathbf{r}_{CoM} is the center of mass

of each cluster [36]. As expected from percolation, the distribution at filling fraction $\phi = 0.22$ approaches a power law, whose exponent is the fractal dimension of the clusters, $d_f = 1.99 \pm 0.02$, which indicates a planar-like geometry, for $\phi \approx 0.2$ (see also the Supplementary Movie `cluster1.mp4`).

Information on the radius of gyration R_s allows us to compute the cluster's correlation length $\xi^2 = 2 \sum_s R_s n_s s^2 / \sum_s n_s s^2$, which upon approaching the critical point ϕ_c is expected to diverge as a power law $\xi \sim |\phi - \phi_c|^{-\nu}$ [36]. Figure 2(a) shows the dependence of the correlation length ξ on the reduced filling fraction $|\phi - \phi_c|/\phi_c$. Our calculations are consistent with power-law behaviors, and from a best fit we obtain $\phi_c = 0.229$ and $\phi_c = 0.204$ for the $L = 200a$ and $L = 100a$, respectively (ϕ_c is expected to be affected by finite-size effects). We find a correlation length exponent $\nu = 1.11 \pm 0.04$.

The divergence of the correlation length at the critical point has important consequences. It means that close to the percolation critical point all correlation functions are scale invariant, and the only relevant degrees of freedom are related to the correlation length ξ . The system is scale invariant. Thus, by first rescaling all distances and then renormalizing the correlation functions, we should obtain an equivalent system, described by the same equations. These are the key ideas of the renormalization group approach [66].

We can now rationalize some of these results by means of a theoretical argument employing a real-space renormalization group (RSRG) calculation of our percolation problem. We consider a cubic lattice in which sites are occupied with probability p and are vacant with probability $q = 1 - p$; we use this lattice to coarse-grain our continuous system; the lattice cells (*i.e.*, the sites) are occupied or empty depending on the occupation of swimmers. Next, we group the cells by forming larger blocks of linear size $b = 2$. The blocks cover the lattice and maintain its original symmetry. These blocks will play the role of renormalized sites. Given that sites in the original lattice are independently occupied with probability p , we must choose a block occupation probability $p' = \mathcal{R}(p)$ in such a way that $\mathcal{R}(p)$ contains the essential physics of our percolation problem [67]. The RSRG approximation consists in taking sites independently occupied with probability p' . Note that percolation involves the formation of an infinite connected cluster, that is, one that spans the entire lattice. It is thus sensible to define a block as occupied if and only if it contains a set of sites such that the block “percolates” by means of planar clusters. This will define $\mathcal{R}(p)$.

Our RSRG rescales the lattice spacing by a factor $b = 2$ in each spatial dimension. Thus, the rescaled blocks contain 8 cells from the original lattice. The correlation length will be rescaled as $\xi' = b^{-1}\xi$, and the correlation length exponent can be found as $\nu = \frac{\ln b}{\ln \lambda}$, where λ is the eigenvalue of the RSRG transformation linearized around the fixed point p_c , $\lambda \equiv \frac{d\mathcal{R}}{dp}(p)|_{p=p_c}$.

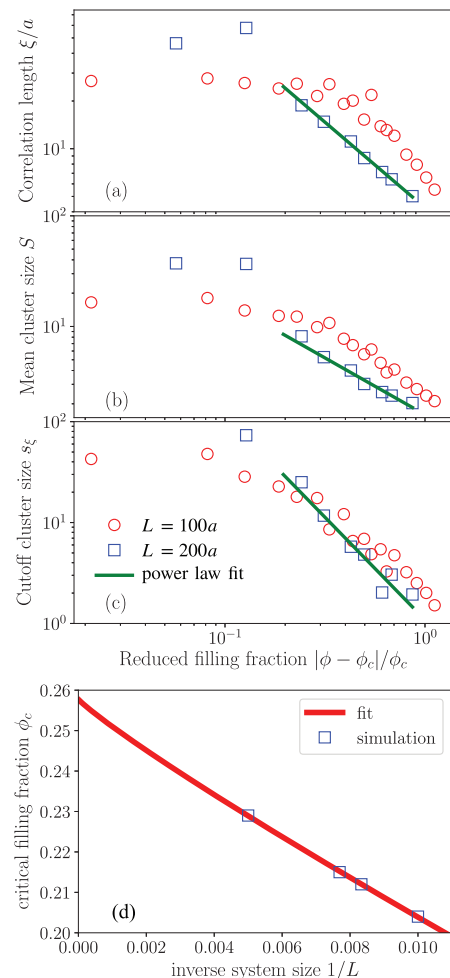


Fig. 2: Dependence of the (a) correlation length, (b) mean cluster size, and (c) cutoff cluster size on the filling fraction ϕ . Solid green lines are power law fits to the data for the $L = 200a$ systems. For (a) the correlation length we find the critical exponent $\nu = 1.11 \pm 0.04$, for (b) the mean cluster size we find the critical exponent $\gamma = 1.05 \pm 0.08$ and for (c) the cutoff cluster size we find the critical exponent $\sigma = 0.49 \pm 0.09$. (d) Critical filling fraction as a function of system size is shown. The fit yields an ordinate intercept 0.2578 ± 0.0005 .

Because the fractal dimension $d_f \approx 2$, in our cubic lattice, a cell is occupied if a planar configuration of sites is occupied. Thus, we only consider configurations of four (tetramers) and three (trimers) particles as our clusters. We now need to count all possible ways to form planar tetramers and trimers. For tetramers, this is equivalent to counting the sides, face diagonals, and body diagonals of a cube, giving a total of 18 configurations. Trimers can be thought of as tetramers with one hole; thus there are 4 ways to place a hole in a tetramer; in total there are 72 configurations. We find

$$p' = \mathcal{R}(p) = 18p^4(1-p)^4 + 72p^3(1-p)^5. \quad (4)$$

We identify p_c with $\phi_c = 0.229$, and we find $\nu \simeq 1.21$. Our RSRG estimate comes relatively close to the value of ν estimated from our simulations.

Further statistical information can be extracted from the mean cluster size $S = \sum_s n_s s^2 / \sum_s n_s s$, which close to criticality scales as $S \sim |\phi - \phi_c|^{-\gamma}$ defining the exponent γ [36]. Figure 2(b) shows the mean cluster size as a function of $|\phi - \phi_c|/\phi_c$. We obtain an optimal critical filling fraction $\phi_c = 0.229$ ($L = 200a$) and $\phi_c = 0.204$ ($L = 100a$). Additionally, we fitted a power law distribution to test the predicted scaling law for S and find $\gamma = 1.05 \pm 0.08$.

Because our simulations are based on finite systems, the growth of the mean cluster size S will be capped once the correlation length $\xi \approx L$; thus S will obey the general scaling $S(\xi, L) = \xi^{\gamma/\nu} s_1(L/\xi)$. Close to ϕ_c , $\xi \gg L$ and we expect $S(\xi, L) \propto L^{\gamma/\nu}$. This is verified by the asymptotic values in fig. 2(b). These results bolster our assumption that the transition we find in our microswimmer system corresponds to a percolation transition.

We can extract another critical exponent from the cutoff cluster size s_ξ , which is also predicted to diverge close to percolation $s_\xi \sim |\phi - \phi_c|^{-\frac{1}{\sigma}}$, thus defining the exponent σ . Figure 2(c) shows the cutoff cluster size for varying reduced filling fraction $|\phi - \phi_c|/\phi_c$. Again, we obtain optimal critical filling fraction $\phi_c = 0.229$ for $L = 200a$, and $\phi_c = 0.204$ for $L = 100a$. A power-law fit yields the critical exponent $\sigma = 0.49 \pm 0.09$.

To investigate the dependence of our results on the finite size of the simulated system, we perform a finite-size scaling by repeating the previous analysis for different system sizes. Figure 2(d) shows the dependence of the critical filling fraction for each simulated system on the inverse system size and a fit to the expected scaling $1/L^\nu$. We find an ordinate intersect 0.2578 ± 0.0005 , which is the critical filling fraction to be expected for an infinite system size.

Using the values of the critical exponents and fractal dimension found so far, we can now apply a more stringent test from percolation theory consisting in the scaling relations [36] $\sigma = 1/(\nu d_f)$, $\gamma = \nu(2d_f - d)$, where $d = 3$ is the dimensionality of the system. The exponents computed from our simulations satisfy to a good approximation the above scaling relations. Taken together, the scaling behavior paint a picture consistent with the presence of a percolation transition in our microswimmer system.

Conclusion. – We have shown that pusher-type microswimmers exhibit a percolation transition at $\phi_c \simeq 0.229$, with a probability distribution approaching a scale-free form. We verified two classical scaling relations from percolation theory. For $\phi > \phi_c$, system-spanning clusters arise. Additionally, real-space renormalization group calculations recover the correlation length critical exponent. As the percolation critical point is approached the correlation length ξ diverges. From this fact self-similarity emerges in the statistical properties of the clusters.

The physical origin of the percolative aggregation discussed here stems from the interplay of steric forces and localized attractive interactions among the microswimmers mediated by hydrodynamic interactions. Our results are

robust for sufficiently large Péclet numbers ($\mathcal{P} \gtrsim 10^2$) enabling strong enough hydrodynamic attractions. Experimental investigations have identified some signatures of heterogeneous dynamics [29,30]. Identifying the existence of a percolation critical point can have strong implications on the understanding of the nature of the fluctuations of microswimmers, and possibly give insight into the transition from planktonic to sessile in surface colonization.

Finally, the critical exponents found in our microswimmer model point differ from the known ordinary-percolation or directed-percolation universality classes. This fact might point to the existence of a new universality class associated to microswimmers interacting through hydrodynamic and steric forces. It is however premature to speak of any universality class associated to microswimmers until more systems are investigated.

We acknowledge support from DFG (SFB 937, A20) and from the Max Planck Society. F-J-S thanks the ICMM group at Loughborough University for the kind hospitality which enabled this work. We are grateful to JAN CAMMANN for useful discussions.

Data availability statement: The data that support the findings of this study are available upon reasonable request from the authors.

REFERENCES

- [1] DORKEN G., FERGUSON G. P., FRENCH C. E. and POON W. C. K., *J. R. Soc. Interface*, **9** (2012) 3490.
- [2] COSTERTON J. W., LEWANDOWSKI Z., CALDWELL D. E., KORBER D. R. and LAPPIN-SCOTT H. M., *Annu. Rev. Microbiol.*, **49** (1995) 711.
- [3] ALLDREDGE A. L. and GOTSCHALK C. C., *Deep Sea Res. Part A: Oceanogr. Res. Pap.*, **36** (1989) 159.
- [4] KJØRBOE T., ANDERSEN K. P. and DAM H. G., *Mar. Biol.*, **107** (1990) 235.
- [5] ELGETI J., WINKLER R. G. and GOMPPER G., *Rep. Prog. Phys.*, **78** (2015) 056601.
- [6] REIN M., HEINß N., SCHMID F. and SPECK T., *Phys. Rev. Lett.*, **116** (2016) 058102.
- [7] LIU Y. and TAY J.-H., *Biotechnol. Adv.*, **22** (2004) 533.
- [8] GUTZEIT G., LORCH D., WEBER A., ENGELS M. and NEIS U., *Water Sci. Technol.*, **52** (2005) 9.
- [9] HALL-STOODLEY L., COSTERTON J. W. and STOODLEY P., *Nat. Rev. Microbiol.*, **2** (2004) 95.
- [10] DOMBROWSKI C., CISNEROS L., CHATKAEW S., GOLDSTEIN R. E. and KESSLER J. O., *Phys. Rev. Lett.*, **93** (2004) 098103.
- [11] SCHWARZENDAHL F. J. and MAZZA M. G., *Soft Matter*, **14** (2018) 4666.
- [12] COPELAND M. F. and WEIBEL D. B., *Soft Matter*, **5** (2009) 1174.
- [13] WIOLAND H., WOODHOUSE F. G., DUNKEL J., KESSLER J. O. and GOLDSTEIN R. E., *Phys. Rev. Lett.*, **110** (2013) 268102.
- [14] ATIS S., WEINSTEIN B. T., MURRAY A. W. and NELSON D. R., *Phys. Rev. X*, **9** (2019) 021058.

- [15] WENSINK H. H., DUNKEL J., HEIDENREICH S., DRESCHER K., GOLDSTEIN R. E., LÖWEN H. and YEOMANS J. M., *Proc. Natl. Acad. Sci. U.S.A.*, **109** (2012) 14308.
- [16] YAZDI S. and ARDEKANI A. M., *Biomicrofluidics*, **6** (2012) 044114.
- [17] HERNANDEZ-ORTIZ J. P., STOLTZ C. G. and GRAHAM M. D., *Phys. Rev. Lett.*, **95** (2005) 204501.
- [18] SOKOLOV A., ARANSON I. S., KESSLER J. O. and GOLDSTEIN R. E., *Phys. Rev. Lett.*, **98** (2007) 158102.
- [19] ZHANG H.-P., BEÁĀŽER A., FLORIN E.-L. and SWINNEY H. L., *Proc. Natl. Acad. Sci. U.S.A.*, **107** (2010) 13626.
- [20] EVANS A. A., ISHIKAWA T., YAMAGUCHI T. and LAUGA E., *Phys. Fluids*, **23** (2011) 111702.
- [21] SOKOLOV A. and ARANSON I. S., *Phys. Rev. Lett.*, **109** (2012) 248109.
- [22] RYAN S. D., SOKOLOV A., BERLYAND L. and ARANSON I. S., *New J. Phys.*, **15** (2013) 105021.
- [23] STENHAMMAR J., NARDINI C., NASH R. W., MAREN-
DUZZO D. and MOROZOV A., *Phys. Rev. Lett.*, **119** (2017) 028005.
- [24] CATES M. E. and TAILLEUR J., *Annu. Rev. Condens. Matter Phys.*, **6** (2015) 219.
- [25] HOELL C. and LÖWEN H., *J. Chem. Phys.*, **144** (2016) 174901.
- [26] EZHILAN B., SHELLEY M. J. and SAINTILLAN D., *Phys. Fluids*, **25** (2013) 070607.
- [27] ALARCÓN F. and PAGONABARRAGA I., *J. Mol. Liq.*, **185** (2013) 56.
- [28] YOSHINAGA N. and LIVERPOOL T. B., *Eur. Phys. J. E*, **41** (2018) 1.
- [29] CHEN D. T. N., LAU A. W. C., HOUGH L. A., ISLAM M. F., GOULIAN M., LUBENSKY T. C. and YODH A. G., *Phys. Rev. Lett.*, **99** (2007) 148302.
- [30] LIU Z., ZENG W., MA X. and CHENG X., *Soft Matter*, **17** (2021) 10806.
- [31] THEURKAUFF I., COTTIN-BIZONNE C., PALACCI J., YBERT C. and BOCQUET L., *Phys. Rev. Lett.*, **108** (2012) 268303.
- [32] BUTTINONI I., BIALKÉ J., KÜMMEL F., LÖWEN H., BECHINGER C. and SPECK T., *Phys. Rev. Lett.*, **110** (2013) 238301.
- [33] PALACCI J., SACANNA S., STEINBERG A. P., PINE D. J. and CHAIKIN P. M., *Science*, **339** (2013) 936.
- [34] MATHIJSEN A. J. T. M., CULVER J., BHAMLA M. S. and PRAKASH M., *Nature*, **571** (2019) 560.
- [35] DOOSTMOHAMMADI A., SHENDRUK T. N., THIJSSSEN K. and YEOMANS J. M., *Nat. Commun.*, **8** (2017) 15326.
- [36] STAUFFER D. and AHARONY A., *Introduction to Percolation Theory* (Taylor & Francis) 2003.
- [37] WENSINK H. H., KANTSLEER V., GOLDSTEIN R. E. and DUNKEL J., *Phys. Rev. E*, **89** (2014) 010302.
- [38] WYSOCKI A., ELGETI J. and GOMPPER G., *Phys. Rev. E*, **91** (2015) 050302.
- [39] OSTAPENKO T., SCHWARZENDAHL F. J., BÖDDEKER T. J., KREIS C. T., CAMMANN J., MAZZA M. G. and BÄUMCHEN O., *Phys. Rev. Lett.*, **120** (2018) 068002.
- [40] COLBERG P. H. and KAPRAL R., *Chem. Phys.*, **147** (2017) 064910.
- [41] WAGNER M., ROCA-BONET S. and RIPOLL M., *Eur. Phys. J. E*, **44** (2021) 1.
- [42] THEERS M., WESTPHAL E., QI K., WINKLER R. G. and GOMPPER G., *Soft Matter*, **14** (2018) 8590.
- [43] LIGHTHILL M. J., *Commun. Pure Appl. Math.*, **5** (1952) 109.
- [44] BLAKE J. R., *J. Fluid Mech.*, **46** (1971) 199.
- [45] YANG Y., ELGETI J. and GOMPPER G., *Phys. Rev. E*, **78** (2008) 061903.
- [46] REIGH S. Y., WINKLER R. G. and GOMPPER G., *Soft Matter*, **8** (2012) 4363.
- [47] DRESCHER K., DUNKEL J., CISNEROS L. H., GANGULY S. and GOLDSTEIN R. E., *Proc. Natl. Acad. Sci. U.S.A.*, **108** (2011) 10940.
- [48] ADITI SIMHA R. and RAMASWAMY S., *Phys. Rev. Lett.*, **89** (2002) 058101.
- [49] SAINTILLAN D. and SHELLEY M. J., *Phys. Rev. Lett.*, **99** (2007) 058102.
- [50] BASKARAN A. and MARCHETTI M. C., *Proc. Natl. Acad. Sci. U.S.A.*, **106** (2009) 15567.
- [51] MALEVANETS A. and KAPRAL R., *J. Chem. Phys.*, **110** (1999) 8605.
- [52] NOGUCHI H., KIKUCHI N. and GOMPPER G., *EPL*, **78** (2007) 10005.
- [53] GÖTZE I. O., NOGUCHI H. and GOMPPER G., *Phys. Rev. E*, **76** (2007) 046705.
- [54] WEEKS J. D., CHANDLER D. and ANDERSEN H. C., *J. Chem. Phys.*, **54** (1971) 5237.
- [55] SCHWARZENDAHL F. J. and MAZZA M. G., *J. Chem. Phys.*, **150** (2019) 184902.
- [56] GUELLE D., BRENNER H., FRANKEL R. B. and HARTMAN H., *J. Theor. Biol.*, **135** (1988) 525.
- [57] FILY Y. and MARCHETTI M. C., *Phys. Rev. Lett.*, **108** (2012) 235702.
- [58] REDNER G. S., HAGAN M. F. and BASKARAN A., *Phys. Rev. Lett.*, **110** (2013) 055701.
- [59] STENHAMMAR J., TIRIBOCCHI A., ALLEN R. J., MAREN-
DUZZO D. and CATES M. E., *Phys. Rev. Lett.*, **111** (2013) 145702.
- [60] SAINTILLAN D. and SHELLEY M. J., *Phys. Rev. Lett.*, **100** (2008) 178103.
- [61] SAINTILLAN D. and SHELLEY M. J., *Phys. Fluids*, **20** (2008) 123304.
- [62] HOELL C., LÖWEN H. and MENZEL A. M., *J. Chem. Phys.*, **149** (2018) 144902.
- [63] BÁRDFALVY D., NORDANGER H., NARDINI C., MORO-
ZOV A. and STENHAMMAR J., *Soft Matter*, **15** (2019) 7747.
- [64] SAFRAN S. A., WEBMAN I. and GRETT G. S., *Phys. Rev. A*, **32** (1985) 506.
- [65] HEYES D. M. and MELROSE J. R., *Mol. Phys.*, **66** (1989) 1057.
- [66] HU B., *Phys. Rep.*, **91** (1982) 233.
- [67] REYNOLDS P. J., STANLEY H. E. and KLEIN W., *J. Phys. C: Solid State Phys.*, **10** (1977) L167.